A constitutive equation for gas hydrate-containing soils considering hydrate morphology and its transition

Hiromasa Iwai[1] and T. Kawasaki[1]

[1] Department of Civil and Environmental Engineering, Nagoya Institute of Technology, Nagoya 466-8555, Japan.

ABSTRACT

It has been found that there are obvious differences in stress-strain relationship and dilatancy behavior between methane hydrate and carbon dioxide hydrate-bearing soils, even if total amount of hydrate content is the same for both. In order to express the mechanical behavior of gas hydrate-bearing soils, several constitutive models for GH-bearing soils have been proposed so far. There are, however, no models that have taken the difference of hydrate morphology into account. In the present study, we propose a new elastoplastic constitutive equation with consideration of the difference of the hydrate morphology, and the proposed model is then applied to the past experimental results. The proposed model well matches the experimental data. It indicates that the difference in the mechanical behavior between methane hydrate and carbon dioxide hydrate can be explained from the viewpoint of the hydrate morphology.

Keywords: constitutive model; methane hydrate; carbon dioxide hydrate; triaxial compression tests

1 INTRODUCTION

Gas hydrates (GHs) have been recognized as an important material for new energy resources and for environmental issues. For example, Methane hydrates (MHs) are expected as a natural gas resource, since a large amount of methane gas trapped inside a cage-like solid structures of MHs. Another example is CO_2-hydrates (CDHs: carbon dioxide hydrate), which has been recognized as a key material for both enhancement of MH-recovery rate and new technology for carbon capture and storage (CCS). In the past decades, many researchers have revealed mechanical properties of MH-bearing and CDH-bearing sediments through both experiments and constitutive modeling. They have indicated that the mechanical properties such as strength, stiffness, and dilatancy behavior of the GH-bearing sediments, in general, increase with increase in hydrate saturation. On the other hand, they have also found that there are obvious differences in the peak strength and the dilatancy behavior between MH and CDH-bearing samples even though they have the same hydrate saturation. (e.g., Hyodo et al., 2014; Miyazaki et al., 2016). Some researchers have pointed that those differences in MH and CDH may come from difference in hydrate morphology, that is, pore-filling (PF) type, load-bearing (LB) type, and cementing (CM) type as shown in Fig. 1(i.e., Waite et al., 2009).

In order to express the mechanical behavior of gas hydrate-bearing soils, several constitutive models for GH-bearing soils have been proposed so far. There are, however, no models that have taken the difference of the hydrate morphology into account. In the present study, we propose a new elastoplastic constitutive equation with consideration of the difference of the hydrate morphology, and the proposed model is then applied to the past experimental results. The proposed model well matches the experimental data.

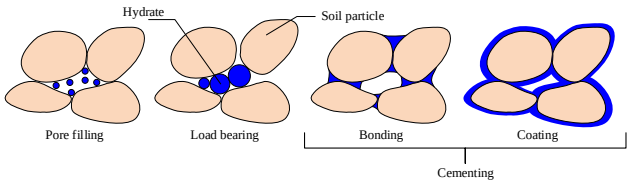

Fig. 1. Schematic view of hydrate morphology and interactions with soil particles.

2 ELASTOPLASTIC CONSTITUIVE MODEL

The proposed model in the present study is based on the methane hydrate critical state (MHCS) model proposed by Uchida et al. (2012). The outline of the proposed model is introduced in the following.

2.1 Basic settings

At first, the total hydrate saturation S_r^H is defined as follows:

$$S_r^H = V^H / V^v \tag{1}$$

in which V^H is the volume of the hydrate, and V^v is the volume of void.

In the proposed constitutive model, we assume that there are three different types of hydrate morphology:

pore-filling (PF) type, load-bearing (LB) type, and cementing (CM) type, and the total hydrate saturation S_r^H is expressed by the sum of the saturation of each hydrate morphology:

$$S_r^H = S_{CM}^H + S_{LB}^H + S_{PF}^H \tag{2}$$

$$S_{CM}^H = \alpha S_r^H,\ S_{LB}^H = \beta S_r^H,\ S_{PF}^H = \gamma S_r^H \tag{3}$$

in which α, β, γ are the ratio of each hydrate morphology with respect to the total hydrate saturation., and the total should be equal to 1.

$$0 < \alpha,\ \beta,\ \gamma < 1\ ,\ \alpha + \beta + \gamma = 1 \tag{4}$$

2.2 Yield function

The yield function is given as follows:

$$f = q^2 + M^2 p' \left[p' - R\left(p_c' + p_{CM}' + p_{LB}' \right) \right] \tag{5}$$

where q is the deviator stress, M is the stress ratio at the critical state of host geomaterial, p' is the mean effective stress, p_c' , p_{CM}' , p_{LB}' are the hardening parameters that expand the original yield function: modified Cam-clay model, and the details of those parameters are explained in the next section. The parameter R is the sub-loading surface ratio proposed by Hashiguchi (1989) and its evolution law is given by:

$$dR = -m_R \left\{ \left(p_c' + p_{CM}' + p_{LB}' \right) / p_c' \right\} \ln R \left| d\boldsymbol{\varepsilon}^p \right| \tag{6}$$

where m_R is a fitting parameter and $d\boldsymbol{\varepsilon}^p$ is the plastic strain increment vector. The schematic drawing of the yield function is shown in Fig. 2.

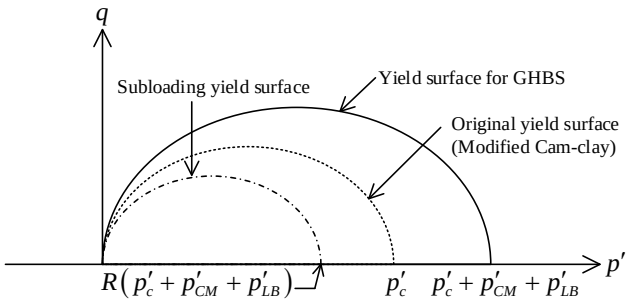

Fig. 2. Schematic drawing of yield function

2.3 Hardening parameters

The hardening parameter p_c' is the conventional consolidation yield stress depending on the plastic volumetric strain $d\varepsilon_v^p$, and the its evolution law is given by:

$$dp_c' / p_c' = (1+e)\, d\varepsilon_v^p / (\lambda - \kappa) \tag{7}$$

(e: void ratio, λ: compression index, κ: swelling index)

In order to express the increase in the strength and the positive dilatancy, we newly introduce two different hardening parameters related to GHs, that is, p_{CM}' and p_{LB}' , because the different hydrate morphology will involve the different hardening behavior. Hence, the p_{CM}' and p_{LB}' are the function of each of the hydrate morphology.

$$p_{CM}' = a_{CM} \left(S_{CM}^H \right)^{b_{CM}} = a_{CM} \left(\alpha S_r^H \right)^{b_{CM}} \tag{8}$$

$$p_{LB}' = a_{LB} \left(S_{LB}^H \right)^{b_{LB}} = a_{LB} \left(\beta S_r^H \right)^{b_{LB}} \tag{9}$$

in which a_{CM} , b_{CM} , a_{LB} , and b_{LB} are the fitting parameters. These parameters are determined so that the material hardening of the CM-type becomes much larger than that of the LB-type.

The hardening parameters will change as the change in the morphology ratio and the total hydrate saturation. In particular, each hydrate morphology ratio will change due to shearing and deformation of void even when the total hydrate saturation is constant. The following two assumptions in regard to the morphology transition are adopted.

First, the CM-type of hydrate morphology changes into the LB-type due to crush and breakage of the hydrates bonding with soils particles as shown in Fig. 3. Thus, the increment of the CM-type ratio α is given by the following equation as depending on the shear strain.

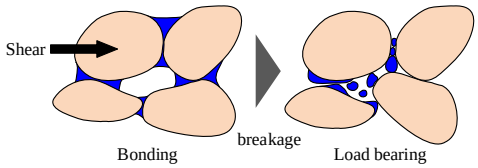

Fig. 3. Morphology transition from CM-type to LB-type

$$d\alpha = -m_\alpha \alpha \left| d\varepsilon_d^p \right| \tag{10}$$

where m_α is a material parameter which determines the transition rate from the CM-type to the LB-type.

Second, the LB-type and the PF-type of the hydrate morphology mutually changes with increase and decrease in the volume of void. The LB-type changes into the PF-type in the case of the volume expansion: positive dilatancy. In contrast, the PF-type changes into the LB-type when it is compression: negative dilatancy. This transition between the LB-type and the PF-type is schematically illustrated in Fig. 4.

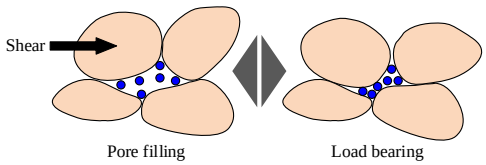

Fig. 4. Morphology transition between LB-type and PF-type

The increment of the PF-type ratio γ is given by the following equation as depending on the plastic

volumetric strain (positive in compression).

$$d\gamma = -m_\gamma \gamma d\varepsilon_v^p \tag{11}$$

where m_γ is a material parameter which determines the transition rate between the PF-type and the LB-type. The increment of the LB-type ratio can be described as the following equation by considering Equation (4), (10) and (11).

$$d\beta = -d\alpha - d\gamma \tag{12}$$

Considering Equation (8)~(12), the evolution laws for the hardening parameters p'_{CM} and p'_{LB} can be given as the following equations.

$$dp'_{CM} = a_{CM} b_{CM} \left(\alpha S_r^H\right)^{b_{CM}-1} \left(\alpha d S_r^H - m_\alpha \alpha \left| d\varepsilon_d^p \right| S_r^H\right) \tag{13}$$

$$dp'_{LB} = a_{LB} b_{LB} \left(\beta S_r^H\right)^{b_{LB}-1} \left\{\beta d S_r^H - \left(d\alpha + d\gamma\right) S_r^H\right\} \tag{14}$$

Finally, by adopting the associated flow rule in the present model, the plastic strain increment vector can be expressed as follows.

$$\left\{d\varepsilon_v^p \quad d\varepsilon_d^p\right\}^T = \Lambda \left\{\partial f / \partial p' \quad \partial f / \partial q\right\}^T \tag{15}$$

3 MODEL APPLICATION

In this section, the performance of the proposed model in the previous section is evaluated by comparing with the past experimental data. The model is applied to the results of drained triaxial compression tests for MH and CDH-bearing sand samples reported by Miyazaki et al.(2016).

3.1 Material parameters

The material parameters used in the analysis are listed in Table 1.

Table 1. Material parameters

Parameters		value
Initial mean effective stress [MPa]	p'_0	1.0
Poisson's ratio	ν	0.2
Stress ratio at the critical state	M	1.17
Compression index	λ	0.16
Swelling index	κ	0.004
Initial void ratio	e_0	0.613
Initial yield stress	p'_{c0}	11.0
Material constant for sub-loading surface	m_R	15.0
Morphology transition parameter (CM to LB)	m_α	1.0
Morphology transition parameter (PF and LB)	m_γ	7.0
Hardening parameter for p'_{CM}	a_{CM}	21.0
Hardening parameter for p'_{CM}	b_{CM}	1.0
Hardening parameter for p'_{LB}	a_{LB}	6.0
Hardening parameter for p'_{LB}	b_{LB}	1.0

3.1 Initial hydrate morphology ratio

In applying the proposed model to the experimental data, the initial ratio of the hydrate morphology is required. It is preferable to determine true initial morphology ratio by visualizing microscopic structures of soil particles and hydrates, however, the initial morphology ratio in the present study is determined so that the constitutive model fits the experimental data. Yoneda et al. (2016) and Jin et al. (2016) are examples of the research on the visualization of GH soil.

Table 2 shows the total hydrate saturation and the initial morphology ratio. In determining the initial morphology ratio, we used the following assumptions based on the past experimental investigations.

(1) All the type of the hydrate morphology, that is, the CM-type, the LB-type and the PF-type, exist at the initial state.
(2) In the MH-bearing soil, the CM-type is more dominant morphology than the LB-type and the PF-type, and the ratio of the CM-type increase with increase in the total hydrate saturation.
(3) In the CDH-bearing soil, the dominant hydrate morphology is set to be the LB-type to express the differences in the strength and the dilatancy between MH and CDH.

In general, the larger strength and the positive dilatancy is observed in the MH-bearing sediments than the CDH-bearing sediments. In addition, it is well recognized that the CM-type strongly enhances the mechanical properties of GH-bearing soils more than the LB-type or the PF-type. That is the reason why the CM-type ratio is larger in MH than CDH as shown in Table 2. The details will be discussed the next section.

Table 2. Total hydrate saturation and initial morphology ratio

MH/CDH	S^H_r	α_0	β_0	γ_0
MH	48.0	0.7	0.2	0.1
MH	34.0	0.5	0.4	0.1
CDH	49.0	0.2	0.7	0.1
CDH	33.0	0.2	0.4	0.4

3.2 Comparison results

The following Fig. 5 indicates a comparison result of the proposed model with the experimental result presented by Miyazaki et al. (2016); they performed a series of drained triaxial compression tests on both the MH and the CDH-containing sand specimens with the total hydrate saturation of about 50%. As previously mentioned, the remarkable point is that both the strength and the positive dilatancy in the MH-bearing sand are greater than those of the CDH, even though the total hydrate saturation is almost the same for both; it is 48.0% in The proposed constitutive model well fitted the experimental results of both the stress-strain relation and the volumetric strain-axial strain relationship by changing the initial morphology ratio.

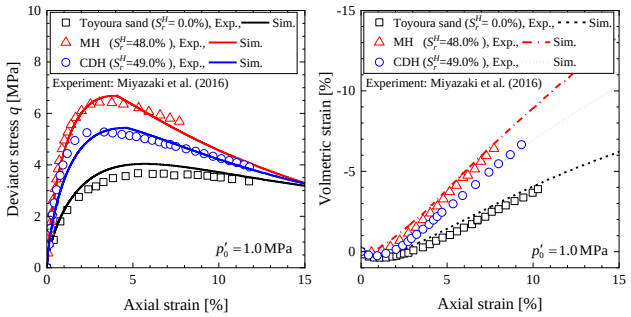

Fig. 5. Comparison of the proposed model and the experimental results with relatively higher hydrate saturation ($S^H_r \cong 50\%$)

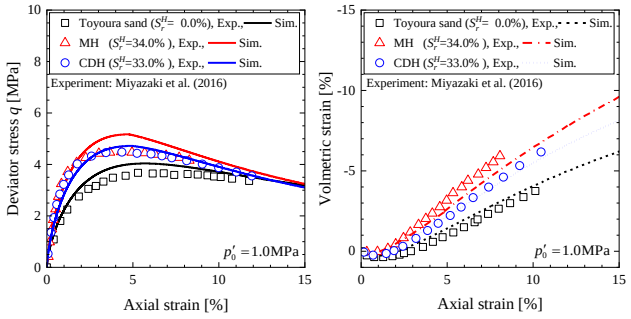

Fig. 6. Comparison of the proposed model and the experimental results with relatively lower hydrate saturation ($S^H_r \cong 33\%$)

Fig. 6 shows the experimental result and the simulation result by the constitutive model for both the MH and the CDH-bearing specimens with lower hydrate saturation: about 30%. In the experimental data, the stress-strain curve becomes almost the same for both MH and CDH-bearing sediments; there is little difference in the strength in the case of the relatively lower hydrate saturation. The volumetric strain, on the other hand, the positive dilatancy is slightly greater in the MH-bearing sample than that of the CDH-bearing sample. In the result of the proposed model, the initial morphology ratio is changed from the previous one with the hydrate saturation of 50% as decrease in the total hydrate saturation. In the MH-bearing sand, for example, the CM-type ratio α decrease from 0.7 to 0.5 with decrease in the total hydrate saturation: from 48.0% to 34.0%. The LB-type ratio β, on the other hand, increase from 0.2 to 0.4 at the same time. Waite et al. (2009) also mentioned that different shear resistance and dilation mechanism occurs at defferent levels of hydrate saturation in pore space; the dominant hydrate morphology changes with change in hydrate saturation. The proposed model well represents both the stress-strain relationship and the volumetric strain curves, while the stress-strain curves of the model is slightly larger than that of the experiment.

4 CONCLUSION

In the present study, a new elastoplastic constitutive model for GH-bearing soils is introduced. The highlight of the proposed model is that the different type of the hydrate morphology is taken into account for the hardening parameters. The model is then applied the past experiment results of the MH and CDH-bearing sand. The main findings obtained from the present study is as follows:

(1) The propose model well fits the stress-strain and the volumetric strain curves for both the MH and the CDH-bearing sand specimen obtained from the past experiment.
(2) The difference between the MH and the CDH can be explained by variation in the initial morphology ratio without changing any other parameter.
(3) The initial ratio of the hydrate morphology changes with change in the total hydrate saturation. The result is consistent with the results obtained from past experimental data.

Since there is still lack of the information on the internal structure of GH-containing sediments, further discussion will be required in determining the actual hydrate morphology ratio.

ACKNOWLEDGEMENTS

This work was supported by JSPS KAKENHI Grant Number JP17K14721.

REFERENCES

Hyodo, M., Li, Y., Yoneda, J., Nakata, Y., Yoshimoto, N., Kajiyama, S., Nishimura, A., Song, Y. (2014). A comparative analysis of the mechanical behavior of carbon dioxide and methane hydrate-bearing sediments. Am. Mineral. 99, 178-183.

Miyazaki, K., Oikawa, Y., Haneda, H., Yamaguchi, T. (2016). Triaxial compressive property of artificial CO_2-hydrate sand. Int. J. Offshore Polar Eng. 26(3), 315-320.

Waite, W.F., Santamarina, J.C., Cortes, D.D., Dugan, B., Espinoza, D.N., Germaine, J., Jang, J., Jung, J.W., Kneafsey, T.J., Shin, H., Soga, K., Winters, W.J. (2009). Physical properties of hydrate-bearing sediments. Rev. Geophys. 47, 1-38.

Uchida, S., Soga, K., Yamamoto, K. (2012). Critical state soil constitutive model for methane hydrate soil. J. Geophys. Res. 117, B03209.

Hashiguchi, K., 1989. Subloading surface model in unconventional plasticity. Int. J. Solids Struct. 25(8), 917-945.

Yoneda, J., Jin, Y., Katagiri, J., Tenma, N., 2016. Strengthening mechanism of cemented hydrate-bearing sand at microscales. Geophys. Res. Lett. 43(14), 7442-7450.

Jin, Y., Konno, Y., Yoneda, J., Kida, M., Nagao, J., 2016. In situ methane hydrate morphology investigation: natural gas hydrate-bearing sediment recovered from the Eastern Nankai Trough area. Energy & Fuels 30(7), 5547-5554.